Interparticle correlations due to electrostatic interactions: A small angle x-ray and dynamic light scattering study. I. Apoferritin

W. Häußler[a)]
Max Planck Institute for Polymer Research, Ackermannweg 10, 55128 Mainz, Germany

A. Wilk and J. Gapinski
Faculty of Physics, A. Mickiewicz University, Umultowska 85, 61-614 Poznan, Poland

A. Patkowski
Max Planck Institute for Polymer Research, Ackermannweg 10, 55128 Mainz, Germany
and Faculty of Physics, A. Mickiewicz University, Umultowska 85, 61-614 Poznan, Poland

(Received 22 December 2000; accepted 4 April 2002)

The structure and dynamics of the spherical protein Apoferritin in aqueous solution are studied over a wide range of protein concentrations and ionic strengths. At high ionic strength and low protein concentration, the intermolecular forces are screened and, therefore, the proteins behave like uncharged molecules. Under these conditions, the form factor of Apoferritin was measured by means of small angle x-ray scattering (SAXS) and the hydrodynamic radius was determined by means of dynamic light scattering (DLS). The sample was found to be highly monodisperse. By decreasing the content of salt added, interactions between the Apoferritin particles were initiated. These intermolecular forces lead to a pronounced maximum in the SAXS intensity. At the same time, a slow mode appears in the relaxation time distribution, additionally to the diffusive mode. The relative amplitudes and correlation times of the diffusive and the slow mode were investigated and compared with predictions of the coupled mode theory. By assuming the slow mode to be related to the correlated motion of ordered domains, the size of these domains was derived from the slow relaxation time. From the x-ray data and the Apoferritin form factor, structure factors of ordered solutions were calculated. The shape of the structure factor peaks was studied as a function of Apoferritin and salt concentration. Finally, by using the DLS information regarding the size of correlated domains, we analyzed the degree of polyelectrolyte ordering within the paracrystalline domains in Apoferritin solutions.
[DOI: 10.1063/1.1481383]

I. INTRODUCTION

Properties of complex fluids strongly depend on the interactions between their components. The time-averaged structure of such fluids is determined by the energy landscape, while the dynamics (Brownian motion of solute molecules) is driven by the thermal energy. Consequently, an interplay between the potential and thermal energy determines the structure and dynamics of these fluids.

In polyelectrolyte solutions, the electrostatic interactions between the polyions and small ions result in an increased complexity of their structural and dynamical properties: A pronounced peak appears in the structure factor and additional dynamic modes contribute to their relaxation spectrum. This complex structural and dynamic picture of the polyelectrolytes can be substantially distorted by polydispersity effects which are usually hard to avoid (especially in synthetic samples) and practically impossible to be corrected for. Thus, high monodispersity of the sample (i.e., identical molecular weight, size, shape, and charge of the polyions) is an important condition for obtaining reliable data suitable for quantitative analysis based on the existing theories. Highly monodisperse samples can be obtained from biological material like DNA,[1–3] tRNA,[4,5] proteins,[6–8] etc.

Ferritin is an iron storage protein, which is found in a variety of animals. It consists of a protein shell surrounding a ferrous core. This protein shell of Ferritin is called Apoferritin ($M_W \approx 450-475$ kD, outer radius approximately 6 nm).[9] It consists of 24 peptide subunits joined through noncovalent interactions. The Apoferritin shell carries a net negative charge at neutral *p*H which ensures its excellent solubility in water.

The structure of the Ferritin core has been the topic of intense study.[10] Its magnetic properties are well known.[11] Due to the iron present in the core, Ferritin is easily observable in electron microscopy.[12] Moreover, the magnetic properties of the Ferritin core allow detection of this protein by means of magnetic imaging methods, which is used in medical examinations (for example, Refs. 13 and 14). Several techniques have been developed to unload and reload the ferrous core.[15]

The protein shell of Ferritin has also been studied using small angle neutron scattering (SANS) as well as synchrotron radiation scattering.[16,17] These studies were restricted mainly to the form factor of the Apoferritin shell. Fewer studies have been undertaken of the interactions between the

[a)]Electronic mail: haeussle@ill.fr

spherical molecules. The aggregation of Apoferritin in solution leading to creation of dimers and multimers has been investigated recently.[9] A couple of years ago, the influence of the salt concentration on the intermolecular distances in adsorbed layers of Apoferritin molecules was studied.[18,19] The effect of oligomers on crystallization of Apoferritin has been studied as well.[20] As an example of interactions with surfaces, the adsorption of Ferritin and the formation of partially ordered two-dimensional arrays were described.[21]

Scarce information has been reported on ordering of Apoferritin in bulk solution. Kilcoyne *et al.* mentioned the appearance of a maximum of the SANS intensity in highly concentrated solution.[16] They analyzed this peak by means of a hard-sphere model. Petsev and Vekilov studied solutions of Apoferritin in NaAC buffer above 10 mM salt content.[22] They conclude that non-DLVO interactions dominate at intermediate concentrations of added salt.

In this paper we present the results of small angle x-ray scattering (SAXS) and dynamic light scattering (DLS)-photon correlation spectroscopy studies of Apoferritin solutions. Our special interest has been focused on the properties of aqueous solutions at low ionic strength. Under these conditions, the protein shell is charged, and the long-range electrostatic interactions between the molecules determine the structure of the solution. Ordering due to electrostatic forces has been studied in various samples. In colloidal solutions, crystalline and liquid-like order appearing as a consequence of hard sphere and electrostatic forces has been reported already several years ago.[23,24] At low ionic strength, a maximum in the scattered intensity is reported. Systematic investigations on latex solutions have been performed, varying the concentration of the latex spheres and the ionic strength.[25] The position of the peak q_{Peak} (=value of the scattering vector at the maximum of the scattered intensity) depends on the concentration of compact polyions in the dilute regime as $q_{\mathrm{Peak}} \sim c^{1/3}$ (or very close to it). In the case of charged spherical colloids, the position and width of the structure factor maximum agrees with theoretical concepts, for example the rescaled mean spherical approximation.[26,27] However, many questions remain still open, for example in the case of nonspherical molecules. Several groups have performed scattering experiments on NaPSS, a charged linear polymer. Similar to colloidal solutions, the structure factor of salt free and low salt aqueous solutions shows a broad maximum.[28–31] In contrast to colloidal solutions, the exponent in the dependence of the position of the maximum on the number concentration varied between 0.3 and approximately 0.5. Contradicting results were reported on the dependence of the peak position on ionic strength.[32,33]

In order to describe the structure factor, de Gennes *et al.* came up with the correlation hole model,[34] while Ise *et al.* proposed an approach to explain the appearance of the maximum in terms of the polyions ordering.[35] Jannink has shown that the Debye–Hückel approximation leads to a structure factor which does not describe the experimental data of solutions of flexible chains.[36] Li and Reed studied the dependence of the peak position on concentration in solutions of Proteoglycan monomers.[37] Boudenne and Francois established a phase diagram for the intermediate concentration regime of acrylamide-acrylic acid.[38] Kassapidou *et al.* reported poor agreement of the experimentally observed polyion structure factor with theory, due to the high linear polyion charge density and, hence, strong electrostatic coupling.[39] Hexagonal packing of charged rods was observed in recent studies.[40,41]

The dynamics of neutral monodisperse polymer solutions studied by means of DLS in the dilute regime is characterized by a single exponential correlation function with a correlation time $\tau = 1/(q^2 D^T)$, where q is the scattering vector and D^T is the translational diffusion coefficient of the polymer. In solutions containing charged polymers at intermediate and low concentrations of added salt the dynamics is much more complex. The diffusive mode depends strongly on the polyion and salt concentration. Two additional modes appear: a fast mode which is related to the diffusion of small ions and the charge fluctuations on the polyion[42,43] and a slow mode which is related to the collective dynamics of correlated polyions (paracrystalline structure, long range order).[1,2,4,44] The slow mode was observed also in semidilute solutions of semiflexible linear polyelectrolytes,[44] but in this case the molecular interpretation is not straightforward. In the case of semiflexible linear polyelectrolytes of a size comparable with $1/q$, the internal modes of the chain contribute to the DLS correlation function both for neutral and charged polymers.[3,45–48]

Theoretical description of the diffusive mode of the polyion is relatively well developed.[42,43] Also the fast dynamics due to the diffusion of small ions and charge fluctuations is included in these theories. There is, however, no sufficient quantitative experimental evidence in support of this description.

The physical interpretation of the slow mode is still controversial mainly because attempts were made to find a universal model valid for both the dilute and semidilute regimes and a poor quality (polydispersity) of some of the samples used in the experiments. The slow mode is not included in the theoretical models. There is, however, mounting evidence that in the case of dilute solutions of compact polyelectrolytes the slow mode can be directly related to the peak observed in the SAXS data and to the dynamics of ordered polyion regions.[1,2,4] Usually, for charged colloidal suspensions the most interesting region for scattering studies is the combination of scattering vector and concentration ranges for which both structure and form factors can be measured in static measurements and, simultaneously, dynamic measurements reveal the diffusion coefficient values in the same q range. Theoretical models based on the Poisson–Boltzmann equation are used to interconnect these results and calculate other properties like hydrodynamic interactions responsible for additional change in the particles diffusivity.[49] The condition to have both static and dynamic data in the same q range comes from the mathematical techniques involved in calculations, mainly Fourier transform. The most interesting q range is the one where a pronounced peak in the static scattering and strong changes of the diffusion coefficient measured by the dynamic experiment are observed.[50] Since this range is defined roughly by the solute number concentration c_n: $q = 2\pi\sqrt[3]{c_n}$, a proper experimental technique has

to be used for a given sample concentration. Additionally, the distance between polyions $(2\pi/q)$ must be small enough, so the electrostatic interactions are relevant. In practice this means that only large colloidal polyelectrolytes of a submicron size can be measured in the interesting q range.

Most of the interesting biological polyelectrolytes (proteins, DNA fragments, tRNA molecules, micelles, small vesicles) are much smaller in size, so the procedures commonly used for colloidal suspensions do not apply in this case because of lack of complementary static and dynamic experimental data in the interesting q range. Diffusion can only be measured using dynamic light scattering in the relatively noninteresting low-q range, while the peak region of the structure factor and decaying part of the form factor are completely out of light scattering q window and have to be measured using x-ray or neutron scattering. It is not clear yet what should be the procedure to combine the results of such experiments performed in different q ranges. Dynamic measurements are, in principle, possible in the q range of the structure factor peak by means of the newly developed method of x-ray photon correlation spectroscopy (XPCS) using synchrotron radiation.[51–53] In practice, however, one is facing severe problems due to low signal level and radiation damage.

Another complication is the earlier mentioned slow mode often observed in the dynamics of small polyelectrolytes[1,2,4,44] in low ionic strength conditions but not predicted by the standard colloidal theoretical models. For example, it is not clear if the q-dependent intensity of the slow mode should be incorporated in the overall $S(q)$ pattern.

The effect of hydrodynamic interactions on the diffusion of small polyelectrolytes in the light scattering q range (close to the $q=0$ limit) can be estimated very roughly on the basis of theoretical colloidal models. The starting point is the dependence $D(q)=D(0)H(q)/S(q)$,[49] arising from appropriate treatment of generalized Smoluchowski equation, where $H(q)$ represents the influence of hydrodynamic interactions on the dynamics of polyions and $D(0)$ is the diffusion coefficient in the absence of interactions. It turns out that for a molecule like Apoferritin in low ionic strength conditions and at moderate concentrations, $H(q)$ can be as small as 0.1 leading to a serious slow-down of the translational diffusion.[54] Thus, the coupled mode theory, which does not take these hydrodynamic interactions into account, might give underestimated values of the effective charge of polyelectrolyte molecules.

As was mentioned before, SAXS measurements of small polyelectrolytes in low ionic strength conditions exhibit a pronounced peak positioned at the q value corresponding to the average distance between the solute molecules at this concentration.[1,2,4,44] Such evidence of liquid-like order stays in contrast to the crystalline order in very dense hard sphere systems, where small aggregates are formed.[55] The main difference lies in packing: densely packed crystalline aggregates (as in colloid crystal) are surrounded by lower concentration solution, while the average distance between small polyions in a low ionic strength solution is the same in the entire sample. One should also be very careful using the concept of "ordered region," because there is no need to have any well defined ordered regions immersed in liquid-like parts of the solution to interpret the static and dynamic experimental data. All we need is a medium-range radial order characterized by a correlation length. The dynamics measured by means of DLS is analyzed using the coupled mode theory. The additional slow mode and the peak observed in the SAXS data from Apoferritin solutions are analyzed in terms of nonideal, paracrystalline ordering within ordered domains.

In the theoretical section (Sec. II), the analysis of the DLS and SAXS data is shortly described, including the principles of the coupled mode theory and the paracrystalline theory. In Sec. III, we describe the preparation of the samples used for the different experimental techniques. Thereafter, we give a brief overview of the experimental techniques applied in this work. The experimental results are presented in Sec. IV, starting with the form factor of Apoferritin molecules. The main part of this work deals with Apoferritin solutions of various protein and salt concentrations. The results of static and dynamic measurements are compared and, finally, used for further analysis of the data. Section V summarizes our conclusions.

II. THEORETICAL BACKGROUND

A. Dynamic light scattering

The time dependent photocount autocorrelation function $g^{(2)}(\tau)$ is measured by means of photon correlation spectroscopy.[45] The relationship between the first order (electric field) autocorrelation function $g^{(1)}(\tau)$ (a Fourier transform of the spectrum) and the second order (intensity) autocorrelation function $g^{(2)}(\tau)$ is given by the Siegert relation

$$g^{(2)}(\tau)=1+|g^{(1)}(\tau)|^2. \tag{1}$$

For a monodisperse solution a single exponential correlation function is expected, with a decay constant Γ, being a relaxation rate of the observed processes. For a polydisperse solution the correlation function can be expressed as

$$g^{(1)}(\tau)=\int_0^\infty \exp(-(\Gamma\tau)G(\Gamma)d\Gamma, \tag{2}$$

where $G(\Gamma)$ is the normalized distribution function of the decay rates. In order to determine $G(\Gamma)$ one has to apply a numerical inverse Laplace transform (for instance by means of the program CONTIN[56]). The average relaxation rate $\overline{\Gamma}$ and the second moment μ_2 of the relaxation rate distribution are defined as

$$\overline{\Gamma}=\int_0^\infty \Gamma G(\Gamma)d\Gamma, \tag{3}$$

$$\mu_2=\int_0^\infty (\Gamma-\overline{\Gamma})^2 G(\Gamma)d\Gamma. \tag{4}$$

The ratio of the second moment to the square of the average linewidth $\mu_2/\overline{\Gamma}^2$ describes the polydispersity of the sample and is called the polydispersity index (PDI). It can be also obtained from a cumulant fit where the correlation function is described by the formula

$$\ln[g^{(1)}(t)] = \ln(A) - \overline{\Gamma}\tau + \frac{\mu_2}{2}\tau^2 - \frac{\mu_3}{6}\tau^3 \tag{5}$$

with μ_2 and μ_3 being the second and the third moments of the distribution, respectively.

The translational diffusion coefficient D^T can be calculated as

$$D = \frac{\Gamma}{q^2}, \tag{6}$$

where q is the absolute value of the scattering vector defined as $q = |\mathbf{q}| = (4\pi n/\lambda)\sin(\theta/2)$, with the solution refractive index n, the laser wavelength λ, and the scattering angle θ.

B. Coupled mode theory

In polyelectrolyte solutions, motion of polyions and small ions is coupled due to electrostatic interactions. The influence of these interactions on the translational diffusion coefficient can be estimated according to the coupled mode theory.[42,45,57–59] The coupling between small ions and polyions is described by the linearized Poisson–Boltzmann equation

$$\Delta\phi(r) = -\frac{4\pi e}{\epsilon_S}[Z_p \Delta n_p'(r,t) + Z_a \Delta n_a'(r,t) + Z_c \Delta n_c'(r,t)], \tag{7}$$

where $\phi(r,t)$ is the electrostatic potential, $\Delta n_j'(r,t)$ is the fluctuation in the number of ion species "j" around its mean value $n_j'(r)$, Z_α is the number of charges on the ion α ($j,\alpha =$ "p": polyion, "a": anion, "c": cation), e is the value of the electron charge and ϵ_S the dielectric constant of the medium. This linearization is correct only if the polyion charge can be treated as a point charge and if $Z_a\phi(r) \ll k_B T$.

The number concentration fluctuates around an average value according to the diffusion equation with an additional term corresponding to the electrostatic interactions

$$\frac{\delta \Delta n_j'(r,t)}{\delta t} = D_j \nabla^2 \Delta n_j'(r,t) + D_j \frac{e Z_j n_j}{k_B T} \nabla^2 \phi(r). \tag{8}$$

The spatial Fourier transform $[\nabla^2 \Delta n_j'(r,t) \rightarrow -q^2 \Delta n_j'(q,t)]$ is given by

$$\left[\frac{\delta n_j'(q,t)}{\delta t}\right] = -[M(q)][n_j'(q,t)], \tag{9}$$

where

$$\Delta n'(q,t)^T = [\Delta n_p'(q,t), \Delta n_a'(q,t), \Delta n_c'(q,t)], \tag{10}$$

and

$$[M(q)] = \begin{bmatrix} D_P(q^2 + \lambda_P^{-2}) & \frac{D_P Z_a}{Z_P \lambda_P^2} & \frac{D_P Z_c}{Z_P \lambda_P^2} \\ \frac{D_a Z_P}{Z_a \lambda_a^2} & D_a(q^2 + \lambda_a^{-2}) & \frac{D_a Z_c}{Z_a \lambda_a^2} \\ \frac{D_c Z_P}{Z_c \lambda_c^2} & \frac{D_c Z_a}{Z_c \lambda_c^2} & D_c(q^2 + \lambda_c^{-2}) \end{bmatrix}. \tag{11}$$

q is the absolute value of the scattering vector, λ_i is the partial contribution to the Debye–Hückel screening parameter for species i:

$$\lambda_i^{-2} = \frac{4\pi e^2}{\epsilon k_B T} \langle n_i' \rangle Z_i^2. \tag{12}$$

The three eigenvalues of the matrix $|[M(q)] - \lambda_i I| = 0$ (with the identity matrix I) represent the normal mode decay rates, with λ_1 being the decay rate of charge fluctuation, independent of the scattering vector, λ_2 the decay rate of polyion diffusion coupled with small ion diffusion and λ_3 the small ion diffusion. The last two decay rates exhibit following dependence on the scattering vector q:

$$\lambda_2 = D_P q^2 + A_1 q^4 + A_2 q^6 + \ldots,$$
$$\lambda_3 = D_s q^2 + B_1 q^4 + B_2 q^6 + \ldots, \tag{13}$$

with D_P and D_s as the polyion and small ion diffusion coefficients, respectively, defined by λ_i/q^2 as $q \rightarrow 0$ and the higher than quadratic terms in q are neglected.

We should note, however, that the coupled mode theory does not take into account hydrodynamic interactions between the molecules, which must lead to some underestimation of the fitted values of particle charge.

C. Paracrystalline theory

The structure factor profile $S(q)$ of partially ordered systems can be described by the three-dimensional paracrystalline theory of Hosemann and Bagchi.[60] While other theories have been developed only for either crystals or liquids, the Hosemann theory represents a more general diffraction theory. Based on this theory, Matsuoka *et al.* calculated paracrystalline structure factor functions for cubic lattices.[61] The shape of the structure factor function is defined by (a) the average distance a between the molecules in the paracrystal lattice, (b) the polydispersity of the ordered particles (because of the small polydispersity of the samples measured, the influence of the polydispersity on the structure factor can be neglected in this case), (c) by the deviations of the particle positions from ideal lattice order, and (d) by the thermally caused fluctuations of the position of the particles. Moreover, $S(q)$ is also influenced (e) by the limited size of the paracrystals. This feature is defined by the correlation of lattice points. Within one microparacrystal of size L (equal for all spatial dimensions), all lattice points are correlated.[61]

At first, we take into account deviations from the ideal crystalline ordering according to permanent disorder and thermal displacement. The function h_1 takes into account these effects for a simple-cubic lattice:[61]

$$h_1(q;a,\Delta a_1,\Delta a_2)=\int\int d\varphi d\Theta \,\mathrm{Re}\left\{\frac{1+\exp[-\frac{1}{2}q^2\Delta a_1^2-iaq\cos(\Theta)]}{1-\exp[-\frac{1}{2}q^2\Delta a_1^2-iaq\cos(\Theta)]}\right\}\mathrm{Re}\left\{\frac{1+\exp[-\frac{1}{2}q^2\Delta a_1^2-iaq\cos(\varphi)\sin(\Theta)]}{1-\exp[-\frac{1}{2}q^2\Delta a_1^2-iaq\cos(\varphi)\sin(\Theta)]}\right\}$$
$$\cdot\,\mathrm{Re}\left\{\frac{1+\exp[-\frac{1}{2}q^2\Delta a_1^2-iaq\sin(\varphi)\sin(\Theta)]}{1-\exp[-\frac{1}{2}q^2\Delta a_1^2-iaq\sin(\varphi)\sin(\Theta)]}\right\}\sin(\Theta)\exp(-q^2\Delta a_2^2) \tag{14}$$

with $q=4\pi/\lambda\sin(\theta/2)$, λ: wavelength, θ: scattering angle, a: mean distance between the macroions in solution with uniformly distributed macroions, Δa_1: standard deviation from the mean distance a, and Δa_2: displacement due to thermal vibrations. The integral can only be calculated numerically.

Now we consider also the influence of the size of the paracrystals. As in powders of small crystals, the width of the SAXS peak of a partially ordered sample increases with decreasing size of the correlated regions. Assuming the ideal ordering within crystals of diameter L, the peak shape can be described by a Gaussian:[62,63]

$$h_2(q_{\mathrm{Peak}},L;q)=\exp\left[\frac{-(q-q_{\mathrm{Peak}})^2}{2\,\mathrm{st}_L^2}\right] \tag{15}$$

with the value of the scattering vector at the peak position q_{Peak} and the standard deviation st_L. This parameter known as the Scherrer width[62] depends not only on the size L but also on the shape of the ordered regions.[63]

In order to combine the effects of imperfect ordering (c,d) and limited size of the domains (e), the Gaussian function h_2 describing the latter effect was convoluted with the function h_1. The convolution was carried out in a two-dimensional numerical computation together with the calculation of h_1.

III. EXPERIMENT

A. Samples

Apoferritin from horse spleen was purchased from SIGMA. The concentration was approximately 51 mg/ml, the sodium salt content approximately 100 mM. In order to decrease the ionic strength, small amounts of Apoferritin solution (3 ml) were dialyzed using 10 kD filters (Millipore ''Ultrafree'') and centrifuged at 7500 g. The dialysis was first done to water and, finally, to aqueous solutions of various salt concentrations (NaCl, purchased from Riedel de Haen, purified to >99.8%). Samples of different protein concentrations were prepared in steps starting from the highest concentration. The concentration was determined by weighting the protein solution before and after dialysis. Additionally, the mass density of the protein solution both before and after dialysis was measured. From the values of the content of the added protein, the mass of the sample after dialysis and the density of the final solution, its concentration in (mg/ml) was determined. These values were checked by means of ultraviolet absorption. Before light scattering measurements, the Apoferritin samples were filtered (Millipore filters, pore size 0.22 μm), filled into the light scattering cells and centrifuged at 7500 g for at least 40 min in order to remove air bubbles.

For the x-ray scattering measurements, 100 μl of the sample solution were poured into glass capillaries of diameters between 0.5 and 1 mm. The transmission through empty capillaries was more than 80% because the glass walls were only 0.01 mm thick.

B. Small angle x-ray scattering

The small-angle-x-ray scattering measurements were performed by means of a Kratky camera (Kratky Compact, A. Paar, Austria). X-ray radiation was produced by a generator (Siemens, Kristalloflex 710H) operating at 35 kV and 10–30 mA. The primary beam was filtered and collimated, resulting in a cross section of 1 mm×50 μm at the sample position and a wavelength of 1.54 Å (Cu K_α). The distance between the sample and the detector was set to 240 mm. We used a one-dimensional position-sensitive detector (N. Braun) with a spatial resolution of 117 μm. The counts were allocated electronically to 512 channels and stored in a PC by means of a multichannel analyzer (Silena). The data were first corrected for solvent and background scattering. Because of the large horizontal beam width the main correction process consisted of desmearing the raw data. Therefore, we used a program based on the Strobl algorithm.[64] Absolute intensities were determined by means of the moving slit method.

C. Ultrasmall angles x-ray scattering

The ultrasmall-angle-x-ray scattering measurements were performed at the European Synchrotron Radiation Facility (ESRF Grenoble, ID10). The primary beam was monochromitized by means of Bragg reflections from a double crystal [diamond (111), $\Delta E/E=6\cdot10^{-5}$]. The energy of the reflected photons was about 8 keV, leading to a mean wavelength of 1.55 Å. The beam was collimated in front of the sample region by means of a 10 μm pinhole. The scintillation detector was mounted at a distance of 2.275 m behind the sample. The detector's slit width was 0.5 mm, its height was 2 mm. Thanks to the small size of the slits, the process of the data desmearing could be neglected for $q>6\cdot10^{-3}$ Å^{-1}. However, for smaller q values, the data were corrected for the influence of the detector's slit size. Moreover, all data were corrected for the background and transmission of the samples. To combine the synchrotron data with Kratky camera measurements, the final intensity values were determined by matching the data in the overlap region of Synchrotron and Kratky data.

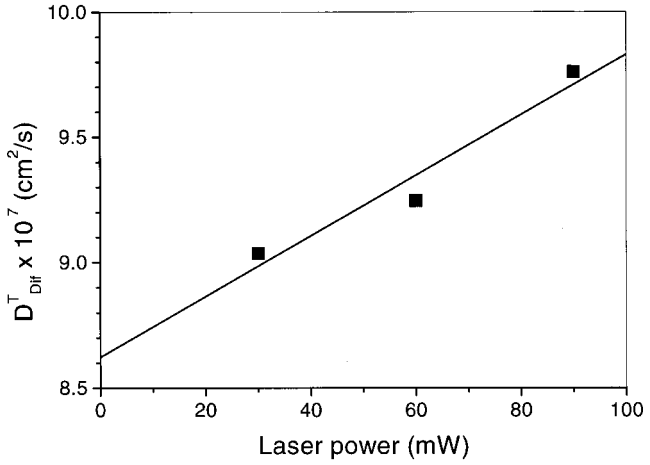

FIG. 1. Translational diffusion coefficient of the polyion diffusive mode D^T_{Dif} in low salt solution of Apoferritin ($c_{\mathrm{Apo}}=36$ mg/ml, 1 mM NaCl) as a function of the incident beam intensity.

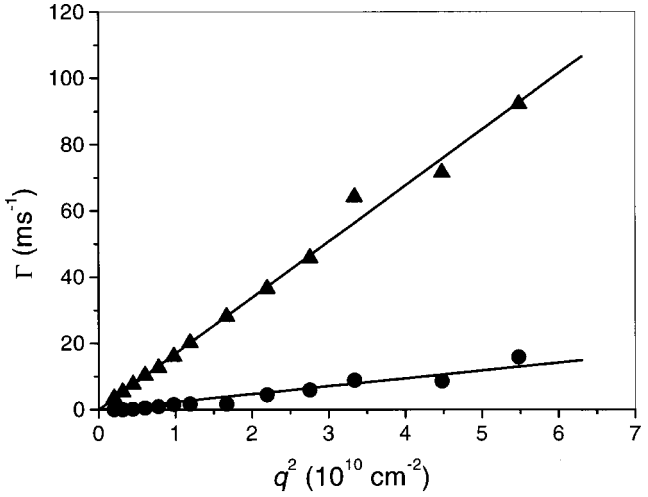

FIG. 2. Angular dependence of the decay rates of the two observed modes (Apoferritin 0.1 mM NaCl, $c=36$ mg/ml). (▲): polyion diffusive mode, (●): slow mode.

D. Photon correlation spectroscopy

The experimental setup for the dynamic light scattering measurements consisted of a Krypton-ion laser (Spectra Physics, USA, $\lambda=674$ nm), a goniometer and a digital correlator ALV-5000E (both from ALV, Langen). An avalanche diode (SPCM-PQ from EG&G, Canada, specially selected) with quantum efficiency more than ten times higher than a conventional photomultiplier tube, was used as a detector. Thus, we were able to perform measurements at much lower incident light intensity. The temperature of the sample was maintained within ± 0.1 °C.

The solutions of Apoferritin at high concentration were placed in a rectangular dust free cell (Hellma, Germany, 45×45 mm^2). To minimize the optical path length of the beam the cell was aligned off-center of the sample holder in such a way that the incident and scattered beam were perpendicular to the cell's walls and their points of incidence were very close to one of its corners. All these precautions were necessary because of residual absorption of the laser light in the solutions at the wavelength used. In order to eliminate the effect of heating (due to absorption) on the measured translational diffusion coefficient D^T, the measurements were performed as a function of the incident beam intensity and the value of D^T extrapolated to zero incident intensity was used for further analysis. A typical dependence of D^T on the laser power is shown in Fig. 1.

The absorption of solutions at low Apoferritin concentrations was very low at the laser wavelength, and the relaxation rates measured did not depend on the incident beam intensity. Such samples were placed in dust-free round cells (10 mm outer diameter) and the q dependence of D^T could be easily measured (see Fig. 2). The relaxation rates for both processes are linear functions of q^2 with the diffusion coefficient as slope. That indicates low polydispersity of the sample and furthermore confirms the diffusive nature of both processes.

IV. RESULTS AND DISCUSSION

A. Sample characterization

The form factor of Apoferritin was the topic under investigation in the first SAXS measurements. Therefore, we used highly diluted aqueous solutions of Apoferritin in water of high salt content. At high salt concentrations, the electrostatic interactions are screened. Furthermore, in highly diluted solutions the intermolecular distances are large and, consequently, the structure factor is constant. Thus, the SAXS data can be described by the form factor of a single molecule.

Apoferritin consists of 24 subunits building a hollow sphere.[10] Thus, the form factor of this protein is given by[65]

$$F^2=\{[\sin(qr_1)-qr_1\cos(qr_1)]-[\sin(qr_2)-qr_2\cos(qr_2)]/[q^3(r_1^3-r_2^3)/3]\}^2 \tag{16}$$

with r_1: outer radius of the sphere, r_2: inner radius of the sphere, and q: absolute value of the scattering vector.

A fit with this function does not give sufficient agreement with the data. While all minimums of the fit function [Eq. (16)] are found at the same height, the data, however, show a systematic decrease of the intensity at the minimum with increasing q. Thus, the high accuracy of the SAXS data makes it possible to determine the polydispersity of the sample. In order to find better agreement with the SAXS data, a fit function was used, which accounts for small deviations from the mean radius of the molecule. Therefore, the form factor was convoluted with a Gaussian distribution. As fit parameters, we chose the mean radius r_1 and the standard deviation Δr_1 of the Gaussian distribution p:

$$p(r_1,\Delta r_1;r)=\exp\left[\frac{(r-r_1)^2}{2\Delta r_1^2}\right]. \tag{17}$$

Furthermore, we took into account the fact that molecules with larger outer radii may show at the same time deviations of the inner radius. Therefore, in addition to the standard deviation of r_1, also the standard deviation Δr_2 was intro-

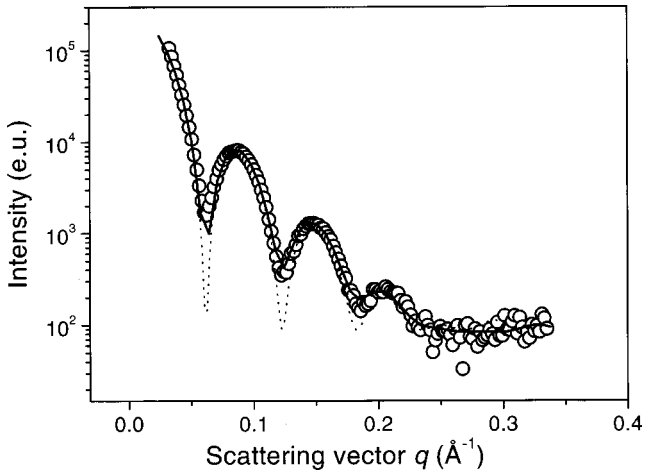

FIG. 3. Apoferritin, 10 mg/ml in 220 mM NaCl. SAXS data (circles) and calculated form factors for hollow spheres with outer radius r_1 and inner radius r_2. Error bars are of the symbols' size. The curve which takes into account a Gaussian distribution of the particles' size (solid line) fits better than the function corresponding to unique particle size (dotted line). The best fit is found for $r_1=(6.11\pm0.02)$ nm and $r_2=(3.75\pm0.02)$ nm with polydispersities $\Delta r_1=3.8\%$ for the outer radius and $\Delta r_1=2.9\%$ for the inner radius.

duced as a fit parameter. The resulting function was found to give good agreement with the data as shown in Fig. 3. The fit gives the following values for radii and radius distributions

$$r_1=(6.11\pm0.02)\ \text{nm}, \quad \Delta r_1/r_1=3.8\%,$$

$$r_2=(3.75\pm0.02)\ \text{nm}, \quad \Delta r_2/r_2=2.9\%.$$

The fit also showed that an increase of the outer radius $r_1+\Delta r_1$ coincides with an increase of the inner radius: $\Delta r_2 \propto \Delta r_1$. This means that deviations of the radii from the mean values have to obey the condition of constant protein shell volume. We think the polydispersity in our shell model simply reflects the irregularities in the shape of the protein shell and probably some breathing motions of the whole molecule.

The DLS time correlation functions for high salt Apoferritin solution were single-exponential with a small value of PDI: 5×10^{-3} (from cumulant analysis). This value indicates an even higher monodispersity in the hydrodynamic radius of the Apoferritin spheres. In contrast to DLS, the SAXS measurements are more sensitive to the size and shape polydispersity. We would like to stress here that relatively high polydispersity reported recently[66] for Ferritin solutions (i) referred to the content of the iron core which may have a molecular weight from zero to as much as the mass of the protein shell and (ii) referred to a sample that was overloaded with iron (on purpose) to the extent inducing aggregation.

While for scattering vectors $q>0.025$ Å^{-1} reliable SAXS data were obtained using the Kratky camera, the scattering at lower q values (USAXS) was investigated using synchrotron radiation at the ESRF in Grenoble. The agreement between the SAXS and USAXS data in the q range of the overlap is very good. Figure 4 presents the results obtained by the two methods against the form factor fit function shown already in Fig. 3.

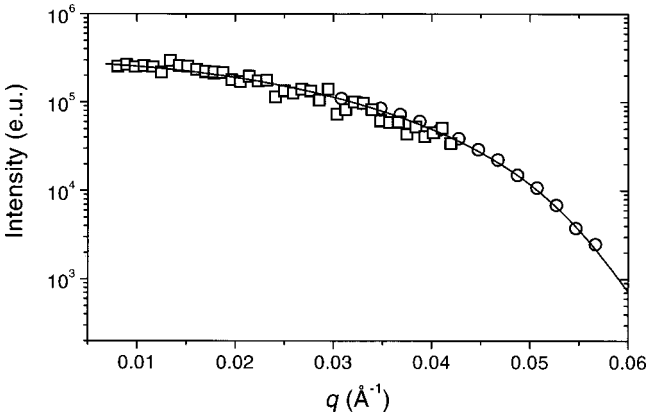

FIG. 4. USAXS data for 10 mg/ml Apoferritin in 15 mM NaCl (squares) are shown together with SAXS data from Fig. 3 (circles) and the best form factor fit to the SAXS data (line). The fit coincides with the USAXS data shown to q values smaller than 0.007 Å^{-1}.

B. Dynamic light scattering

Homodyne photon autocorrelation functions were measured for Apoferritin solutions at various scattering vector lengths, ionic strengths (various NaCl concentrations: 100, 1, 0.1, and 0.01 mM) and over a wide range of Apoferritin concentrations (from 0.1 to 400 mg/ml). At high salt concentrations, the correlation functions exhibit a single exponential behavior as it was described earlier. At lower ionic strength, two well-separated modes are observed in the distribution of the relaxation times obtained by CONTIN[56] (Fig. 5). The first one corresponds to diffusive motion of the polyions, while the second one—considerably slower and consequently called the ''slow mode''—is related to the dynamics of ordered polyion regions. The slow mode is observed for all concentrations of the low salt Apoferritin solutions (1, 0.1, and 0.01 mM NaCl) studied.

Figure 6 shows two correlation functions for different Apoferritin concentrations and their relaxation time distributions obtained from the CONTIN analysis. The relative amplitude of the slow mode increases with increasing the protein concentration, whereas the amplitude of the polyion diffusive mode decreases. The relative amplitudes of both the slow

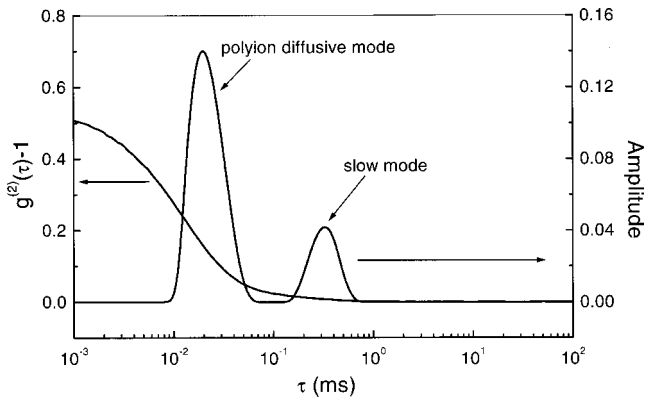

FIG. 5. A typical correlation function measured at low ionic strength of 0.1 mM NaCl at $c_{\text{Apo}}=36$ mg/ml, $\theta=90°$, and $T=20$ °C. As a result of the CONTIN analysis there are found two well separated modes: the polyion diffusive mode and the slow mode.

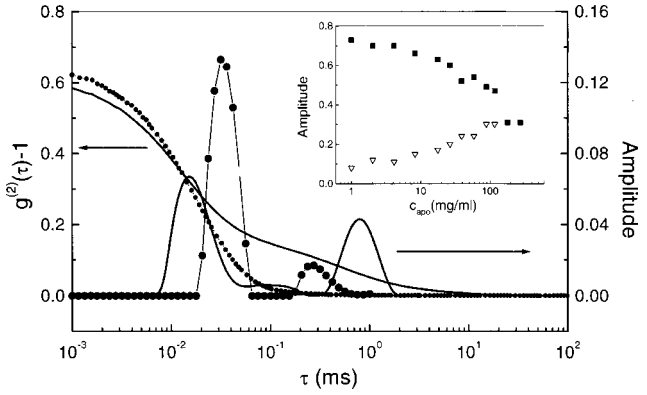

FIG. 6. Correlation functions measured at $\theta=90°$ for different Apoferritin concentrations at constant ionic strength of 0.01 mM NaCl with corresponding relaxation time distributions (line: 234 mg/ml, symbols: 17.6 mg/ml). Inset: relative amplitudes of the polyion diffusive mode and slow mode plotted vs Apoferritin concentration. (■): amplitude of the polyion diffusive mode, (▽): amplitude of the slow mode (Apoferritin 0.1 mM NaCl, $\theta=90°$).

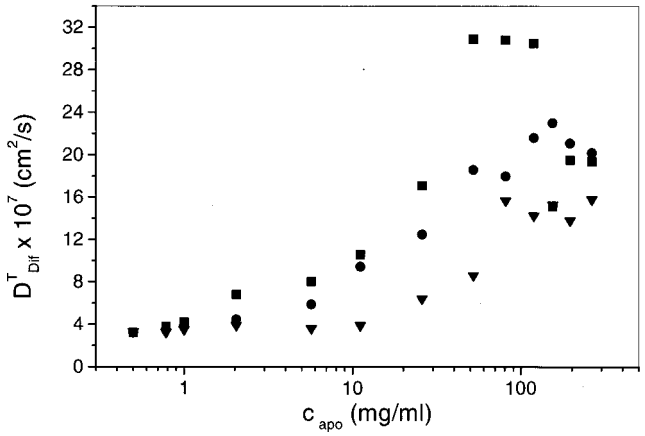

FIG. 8. Concentration dependence of the apparent diffusion coefficient of Apoferritin solutions. The measurements were carried out at scattering angle $\theta=90°$ and at different ionic strengths; (▼): 1 mM NaCl, (●): 0.1 mM NaCl, (■): 0.01 mM NaCl.

mode and the polyion diffusive mode (defined as the amplitude of the process divided by the sum of amplitudes of both processes) are determined from the double exponential fit and are shown as a function of concentration in the inset of Fig. 6. The same effect of the increase of the slow mode amplitude and the simultaneous decrease of the polyion diffusive mode amplitude is observed while decreasing the ionic strength at constant Apoferritin concentration (Fig. 7). The relaxation time of the fast process is getting shorter with both increasing the protein concentration and decreasing the salt content (Figs. 6, 7, and 9). The relaxation time of the slow mode increases with increasing Apoferritin or decreasing salt concentration (see Figs. 6 and 7). The same behavior of the slow mode was reported in the solution of 20-mer DNA.[2]

The relaxation rates obtained from CONTIN analysis and from double-exponential fits were consistent within the experimental error. Translational diffusion coefficients were calculated according to Eq. (6) for $q=1.827\times10^5$ cm^{-1} and Γ was calculated from double exponential fits. The concentration dependence of the translational diffusion coefficient for Apoferritin in solutions of different ionic strengths is shown in Fig. 8, whereas Fig. 9 presents its dependence on the ionic strength at a constant protein concentration.

In general, at low polymer concentrations the dependence of the translational diffusion coefficient on the polyelectrolyte concentration c is linear[1]

$$D(c)=D_0(1+k_Dc+\ldots), \tag{18}$$

where D_0 is the translational diffusion coefficient at zero polymer concentration, k_D is the so-called diffusion second virial coefficient (it characterizes the dependence of the diffusion coefficient on the particular properties of the sample: molecular weight, partial specific volume, etc., and conditions in the solution). The translational diffusion coefficient for noninteracting Apoferritin molecules was obtained by extrapolating the linear dependence of D^T on Apoferritin concentration to zero Apoferritin concentration. Regardless of the ionic strength the same result was obtained: $D_0^T=3.1\times10^{-7}$ cm^2/s. The Stokes–Einstein equation for rigid spheres gives the relationship between the diffusion coefficient at infinite dilution D_0 and hydrodynamic radius r_H:

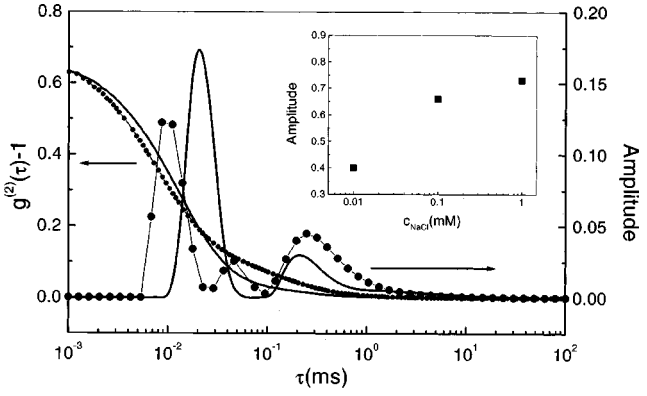

FIG. 7. Correlation functions and CONTIN time distributions measured for different salt concentrations at a constant Apoferritin concentration of 100 mg/ml [line: 1 mM NaCl, (●): 0.01 mM NaCl]; $\theta=90°$. Inset: (■): dependence of the diffusive mode amplitude on the ionic strength at a constant protein concentration of 10 mg/ml ($\theta=90°$).

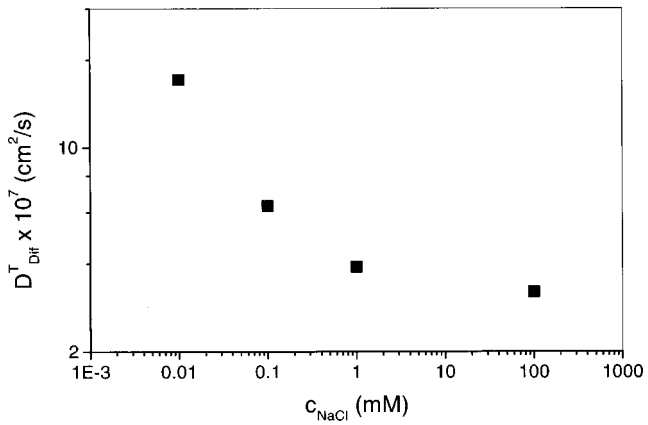

FIG. 9. Ionic strength dependence of the apparent diffusion coefficient at constant Apoferritin concentration of 10 mg/ml.

TABLE I. Parameters used in the CMT calculation.

Item/quantity	Value	Unit
q-scattering vector length	$1.827\times10^{+5}$ (at $\theta=90°$)	cm^{-1}
D_p—apparent diffusion coefficient of Apoferritin[a]	3.1×10^{-7}	$cm^2\,s^{-1}$
D_c—diffusion coefficient of cations (Na^+)[b]	1.1×10^{-5}	$cm^2\,s^{-1}$
D_a—diffusion coefficient of anions (Cl^-)[b]	1.7×10^{-5}	$cm^2\,s^{-1}$
Z_c—charge on cations	1	e
Z_a—charge on anions	-1	e
Z_P—charge on Apoferritin	-2, -3, -4, -5, -6, etc.	e
c_p—concentration of Apoferritin	c_{Apo}	M
c_a—concentration of anion	$c_{\mathrm{NaCl}}=(1,0.1,0.01)\times10^{-3}$	M
C_c—total concentrations of cations	$C_c=\lvert Z_a\rvert c_a+\lvert Z_p\rvert c_p$	M

[a]Diffusion coefficient measured as a function of Apoferritin concentration extrapolated to zero concentration.
[b]Experimental data from [J. H. Wang and S. Miller, J. Am. Chem. Soc. **74**, 1611 (1952)] converted to 20 °C.

$$D=\frac{kT}{6\pi\eta R}, \tag{19}$$

with k_B: Boltzmann constant, T: absolute temperature, and η: solvent viscosity. Thus, the hydrodynamic radius obtained from the experimental value of the diffusion coefficient amounts to 6.9 nm, which is in good agreement with the previously published value of 7.0 ± 0.1 nm.[66,67]

C. Coupled mode theory

The coupled mode theory (CMT) calculations were performed using the input parameters listed in Table I. Figure 10 shows the procedure of determination of the best fit charge indicated in the figure from experimental results. The main graph presents CMT predictions for the whole range of the concentrations studied, whereas the fit for the lowest values is shown in the inset. In order to compare the protein amount with the amount of counterions at different salt content, the protein number concentration was calculated from the weight concentration. At Apoferritin concentrations below 10–50 μM, the CMT fit function describes the dependence of the diffusion coefficient on the concentration well, while the experimental results and CMT predictions are inconsistent at higher concentrations. However, this is not surprising, since under these conditions the particles are so close that the condition of point charge, upon which the coupled mode theory is built, is no longer fulfilled. Moreover, the concentration dependence of hydrodynamic interactions (difficult to estimate) definitely modifies not only the amplitude but also the shape of changes of D_T as a function of polyelectrolyte concentration. Apoferritin has 624 negative and 576 positive dissociable groups. Our measurements were performed in solutions of pH 5.1–5.3. Under comparable conditions, partial dissociation of the protein leading to a net charge of approximately 24 e has been reported in Ref. 22.

D. SAXS and USAXS

The x-ray data measured for samples of very low salt content (0.01 mM NaCl) are shown in Fig. 11. Between $q=0.02$ Å^{-1} and $q=0.045$ Å^{-1}, a pronounced peak is observed for various Apoferritin concentrations from 30 to 259 mg/ml. This peak is due to ordering of the protein molecules in solution. Because the latter are charged, there exists a minimum of the potential energy at definite interparticle distance, which is determined by the respective protein concen-

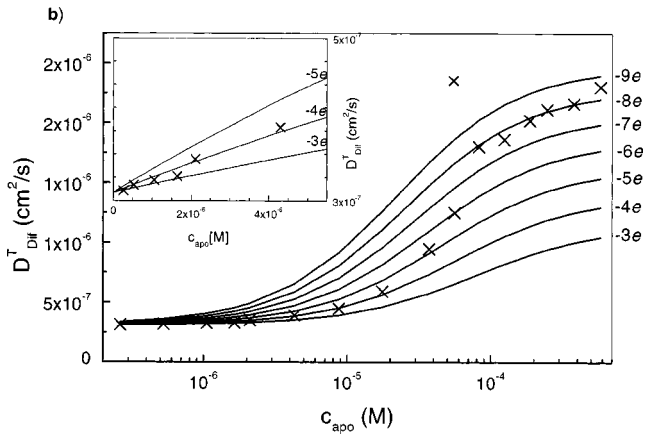

FIG. 10. Determination of the best fit charge from a CMT fit to the experimental results for Apoferritin at 0.1 mM NaCl. (×): experimental values, (lines): coupled mode theory fits for different effective charges indicated at the y axis. Inset: range of the smallest concentrations.

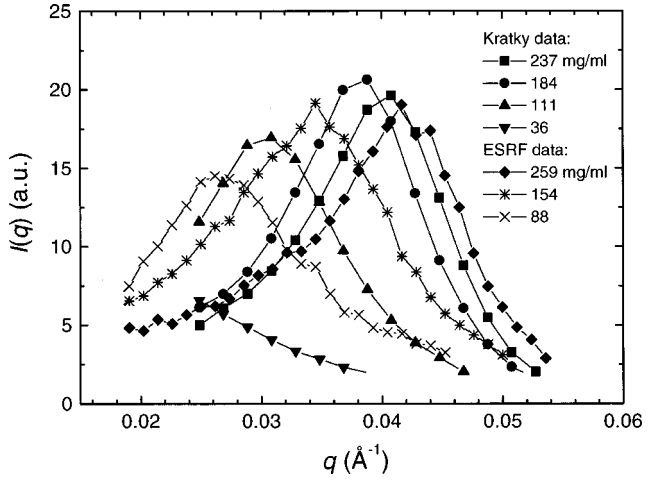

FIG. 11. X-ray data measured for Apoferritin samples at very low salt concentration (0.01 mM NaCl). The data show a pronounced peak between $q=0.02$ Å^{-1} and $q=0.045$ Å^{-1} for Apoferritin concentrations between 30 and 259 mg/ml.

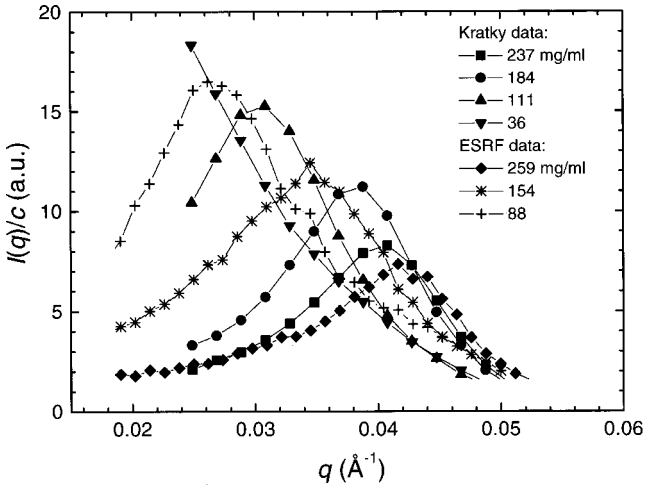

FIG. 12. Data from Fig. 11 scaled with the Apoferritin concentration.

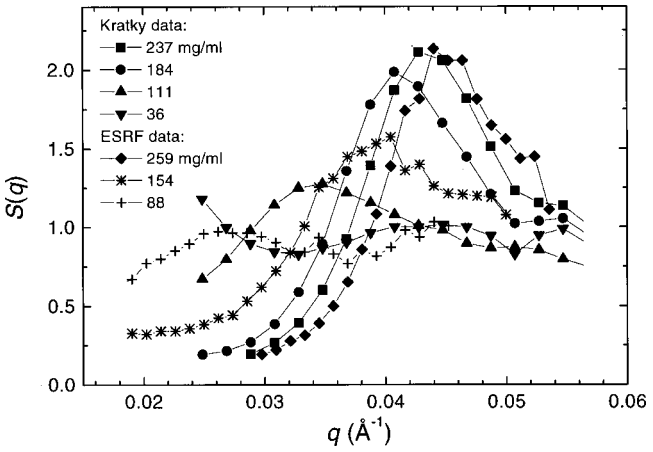

FIG. 13. Structure factor data for different Apoferritin concentrations. The data correspond to the SAXS data shown in Fig. 12. The intensity data divided by the form factor give the structure factor $S(q)$.

tration. From the position of the peak q_{Peak} the average interparticle distance d can be estimated using the Bragg relation $q_{\mathrm{Peak}}=2\pi/d$. Figure 11 shows that the peak shifts to higher q values with increasing protein concentration. As we show later, the peak position of the $I(q)$ spectrum may be shifted by several factors. Nevertheless, this correction is smaller then the tendency observed in the whole concentration range. The height of the maximum increases and the width of the peak decreases with increasing polymer concentration. Furthermore, at very low protein concentrations the peak disappears. Summarizing, with increasing Apoferritin concentration and decreasing interparticle distances we find increasing paracrystalline order in solution.

The SAXS intensity shown in Fig. 11 depends on both the structure factor $S(q)$ resulting from the interparticle ordering and on the form factor of Apoferritin $F^2(q)$. For spherically symmetric particles these two contributions to the scattering cross section can be separated easily, because the scattering curve is given by the product of the form factor and the structure factor[65]

$$\frac{d\sigma}{d\Omega}(q)\propto F^2(q)S(q). \tag{20}$$

In order to properly compare the curves presented in Fig. 11, one should also take into account the number of scattering molecules in the x-ray beam. This simple concentration scaling leads to a picture shown in Fig. 12 with a rather nonintuitive result of peaks' height decreasing with increasing Apoferritin concentrations. The obvious reason for that is the relatively steep negative slope of the Apoferritin form factor, which damps peaks positioned at higher q values, i.e., for more concentrated samples. The data from Fig. 12, but now after having been divided by the form factor are shown in Fig. 13. The plot again exhibits maximums consistent with the peaks of Fig. 12. The main difference between the intensity data (Fig. 12) and the structure factor data (Fig. 13) is the relative height of the peaks and the raised right wing of the $S(q)$ curves. The height of the maximums of the structure factor increases with increasing protein concentrations, as expected.

Moreover, the maximums are shifted slightly to higher q values which is also due to the negative slope of the form factor in the q range under consideration.

Figure 14 shows the SAXS peak at similar protein concentrations as before, but now at 5 mM added salt concentration. Again the SAXS peak is found to be shifted to lower q values and to become broader with decreasing Apoferritin concentration.

All peaks of comparable protein concentration are found to be lower and broader for 5 mM salt solution than 0.01 mM solution. This observation indicates a lower degree of ordering. We can easily explain this behavior taking into account the forces between the negatively charged proteins as in solutions of higher salt content the electrostatic forces between the molecules are screened.

Figure 15 show the Bragg spacing d plotted as a function of protein number concentration for Apoferritin solutions at 0.01 mM NaCl. The Bragg spacing d was calculated from the positions of peak maximums both of the scattering curves $I(q)$ and structure factor profiles $S(q)$. The ideal Bragg spacing (crystal) scales with the average interpolyion distance: $d=c_N^{-1/3}$, where c_N is the number concentration of the protein (solid line in Fig. 15). This formula is expected to hold for a spatially uniform distribution of the macromol-

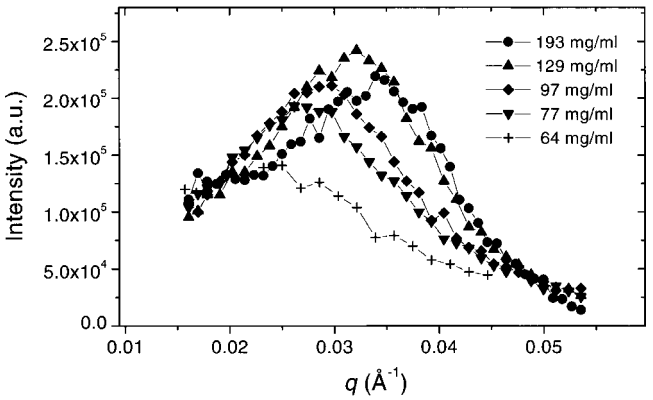

FIG. 14. The SAXS peak at Apoferritin concentrations between 64 and 193 mg/ml and at 5 mM added salt concentration.

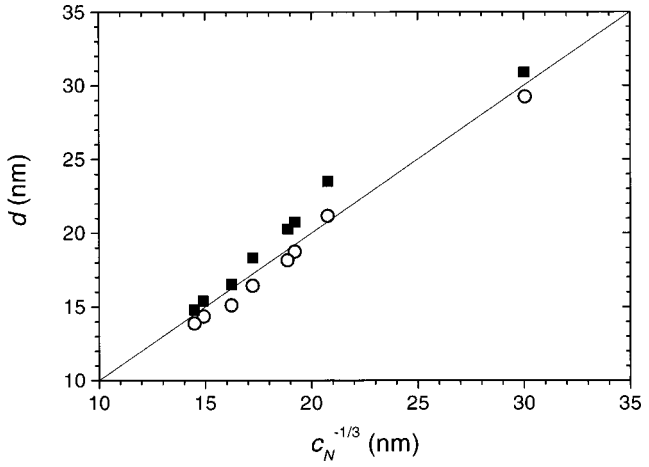

FIG. 15. The Bragg spacing d is calculated from the peak position of the scattering curve (full squares) and the structure factor (open circles) and plotted as a function of the protein concentration. The solid line shows the Bragg condition for a crystal, where d scales with the average interpolyion distance $c_N^{-1/3}$, with c_N being the number concentration of the protein.

ecules in all three dimensions. It is clearly seen in Fig. 15 that both sets of experimental points [d calculated from $I(q)$ and $S(q)$] follow the Bragg condition in terms of the exponent 1/3, but they remain outside the ideal Bragg condition on opposite sides of it. The shift is relatively small and slightly dependent on the way of estimation of the peak position. Due to some asymmetry of the SAXS curves, standard fitting models like Lorentzian or Gaussian will give peak positions shifted to smaller q values (resulting in larger d). The same dependence of the peak position was determined for higher ionic strength of the solution. However, there was no SAXS maximum resolvable for both low protein concentrations and high ionic strength. Therefore, we show the plot for the lowest ionic strength data measured (0.01 mM NaCl), where the described dependence can be observed in a wide range of protein concentrations (36–259 mg/ml).

At constant Apoferritin concentration, the SAXS peak is found to decrease and broaden with increasing salt concentration (Fig. 16). As mentioned earlier, this is due to partial screening of the polyion charge by the added salt which weakens the interactions between polyions and the degree of order in solution. Remarkable influence on the peak width is

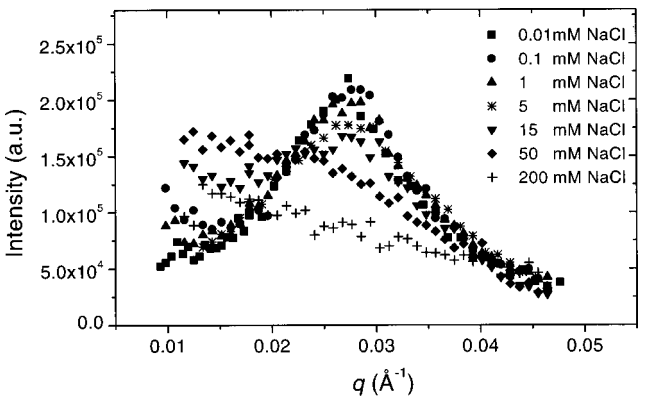

FIG. 16. The SAXS peak at the constant protein concentration of 80 mg/ml for different added salt concentrations as indicated in the figure.

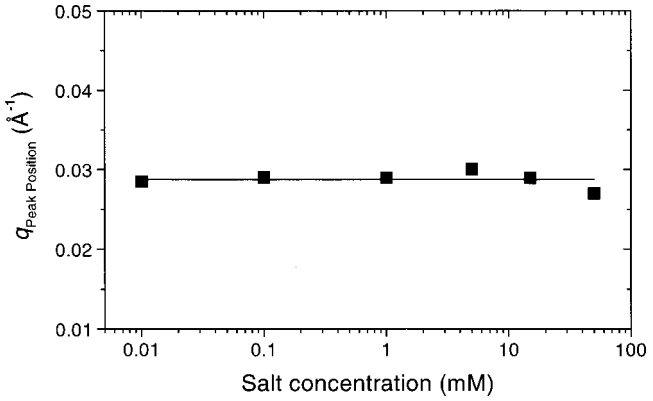

FIG. 17. The q value of the SAXS peak at constant polymer concentration for different salt concentrations.

found at salt concentrations higher than 5–10 mM. For NaCl concentrations above 50 mM, no peak could be seen any more. At salt concentrations of more than 200 mM, any further increase of the salt content has no remarkable influence on the shape of the scattering curve. Moreover, the x-ray data for solutions with high salt and protein concentration of 80 mg/ml do not differ from the form factor measured at the same salt concentration but lower protein concentration (10 mg/ml, see Fig. 11). Finally, from Fig. 17 it can be easily recognized, that the position of the SAXS peak at a constant polymer concentration does not depend on the concentration of salt added.

E. Paracrystalline theory

In order to estimate quantitatively the degree of ordering within Apoferritin solutions at low ionic strength, we analyzed the SAXS data with the paracrystalline theory of Hosemann and Bagchi[60] (Sec. II C). In this theory the width of the peak depends on the spatial and thermal disorder as well as on the size of the ordered region. We assume that the size of the ordered regions may be estimated by means of the results of DLS measurements (Sec. III B). Both DLS and SAXS measurements were performed on the same samples. The slow mode's time scale was about 5–10 times larger than that of the diffusive mode.

The size of the ordered domains L was estimated from the diffusion coefficient of the slow mode in two ways: (i) The hydrodynamic correlation length of the slow mode R_{SE} was directly calculated using the Stokes–Einstein relation and $L_{SE}=2R_{SE}$. (ii) Another way to estimate the correlation length of the ordered region is to calculate a diameter of an ensemble of correlated partially ordered Apoferritin molecules which has a diffusion coefficient equal to that of the slow mode. Unfortunately, there is no procedure to calculate a diffusion coefficient of a dynamically changing ensemble of spheres. The best we can do is to use procedures to calculate a diffusion coefficient of an ensemble of spheres with fixed relative positions.

We simulated an ensemble of ordered spheres (of a radius $r=6.9$ nm) placed at a distance a (defined earlier). The diffusion coefficient of such an ensemble was calculated using the procedure applied extensively in the so-called bead

modeling of biological molecules (see, e.g., Ref. 68 and our recent work[69]). In this way we were able to estimate the radius of this ensemble R_{sim} and the size of the ordered domains $L_{sim}=2R_{sim}$ which have a diffusion coefficient corresponding to the relaxation time of the slow mode. Since in the model applied here it is only the positions of the centers of polyions that define the paracrystal, we defined R_{sim} as the distance from the domain center to the centers of the beads from the outer layer. For the 237 mg/ml Apoferritin solution in 0.01 mM NaCl, using the diffusion coefficient of the slow mode shown in Fig. 6 we obtained $L_{SE}=91$ nm and $L_{sim}=90$ nm (an ensemble of 123 spheres) while for 111 mg/ml Apoferritin solutions at the same NaCl concentration $L_{SE}=86$ nm also in a reasonable agreement with $L_{sim}=84$ nm (an ensemble of 63 spheres). As we can see, both estimates of the size of the ordered regions are practically identical and we can conclude that the hydrodynamic diameter of the slow mode is a good estimate of L at that high concentration. Performing the same kind of calculations for lower protein concentrations we get $L_{sim}/L_{SE}=1.04$ for 80 mg/ml and 1.17 for 10 mg/ml, which is a rather nonintuitive result and, hence, worth mentioning. Bead model calculations show that even relatively hollow structures (below 10% volume fraction) diffuse not much faster than a solid sphere of the same size. This is partially caused by the definition of R_{sim} which does not take into account the size of the bead. For the Apoferritin sample at 237 mg/ml the bead radius is about 15% of the domain radius so the ''real'' simulated domain size for this sample is about 104 nm. Nevertheless, the arguments presented earlier extend the regime of applicability of the $L_{SE}=L$ approximation practically to all Apoferritin concentrations where SAXS peak was observed. The size of the ordered regions is about $L\approx 50$ nm in the highest ionic strength solutions which show the presence of the slow mode, and up to $L\approx 100$ nm in lowest ionic strength solutions with high Apoferritin concentration. Small angle x-ray scattering from an ideal crystal of this diameter would lead to a full width at half maximum (FWHM) β of the peak[62,63]

$$\beta=2\pi/L=0.006-0.013\ \text{Å}^{-1}.$$

However, the width (FWHM) of the SAXS peaks found by a Gaussian fit is between 0.012 Å^{-1} for low salt solutions and 0.023 Å^{-1} for higher salt solutions. Consequently, the limited size of the ordered domains can only partly explain the peak width. Deviations from ideal crystalline ordering and the thermal disorder influence the peak width strongly. In order to deduce correct values of the model parameters describing the spatial disorder, the size of the ordered regions has to be taken into account. Thus, we convoluted the paracrystalline structure factor h_1 [Eq. (14)] with the Gaussian h_2 [Eq. (15)], as described earlier (Sec. II C). The mean distance between two molecules a, the spatial disorder Δa_1, and the thermal disorder Δa_2 were taken as fit parameters. The width st_L of the Gaussian h_2 was calculated as $4/3\times 0.425\ \beta$ and fixed during the fit procedure. The factor 4/3 arises from the assumed spherical shape of the ordered region,[62] and the number 0.425 transforms FWHM into standard deviation of a Gaussian line.

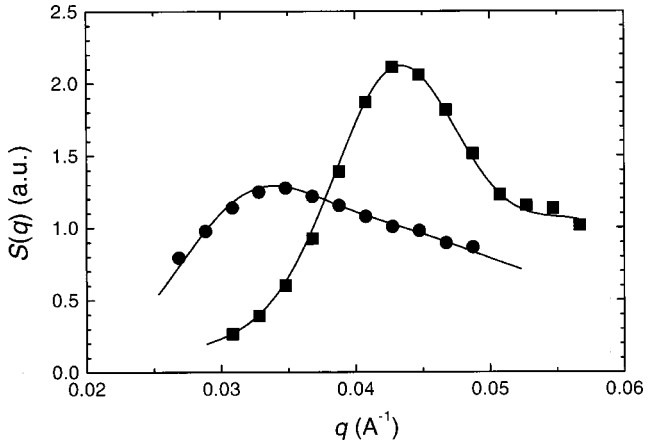

FIG. 18. Structure factor for 237 mg/ml (squares) and 111 mg/ml (circles) Apoferritin solutions at 0.01 mM NaCl. The lines depict the best fit with function h_1 [Eq. (14)] convoluted with the Gaussian h_2 [Eq. (15)] which takes into account the size of the ordered domains. The best fit parameter values are: 237 mg/ml: $a=14.9$ nm, $\Delta a_1=1.8$ nm, $\Delta a_2=1.5$ nm (for $\beta=0.069\ \text{nm}^{-1}$). 111 mg/ml: $a=19.4$ nm, $\Delta a_1=2.5$ nm, $\Delta a_2=1.5$ nm (for $\beta=0.073\ \text{nm}^{-1}$).

The best fit of the functions given in Eqs. (14) and (15) to those SAXS data for two solutions of Apoferritin concentration of 237 and 111 mg/ml at 0.01 mM NaCl are shown in Fig. 18. The values of the fit parameters obtained for the higher polymer concentration are

$$a=(14.93\pm 0.2)\ \text{nm},\quad \Delta a_1=(1.8\pm 0.2)\ \text{nm},$$

$$\Delta a_2=(1.5\pm 0.2)\ \text{nm},\ (\text{for}\ \beta=0.069\ \text{nm}^{-1}).$$

The distance of $a=14.93$ nm is in good agreement with the mean distance of particles so calculated from the Apoferritin concentration a_{conc}, where the average of the literature values (450 kD–475 kD)[9] has been taken as molecular weight

$$a_{conc}=(463\ \text{kg/mol}/237\ \text{g/l}))^{1/3}=14.79\ \text{nm}.$$

For the lower Apoferritin concentration the following values of the fit parameters were obtained:

$$a=19.4\ \text{nm},\quad \Delta a_1=2.5\ \text{nm},$$

$$\Delta a_2=1.5\ \text{nm},\ (\text{for}\ \beta=0.073\ \text{nm}^{-1}).$$

The uncertainty of the numbers for the fit parameters is comparable with the numbers given in the former case. The distance $a=19.4$ nm is in good agreement with the mean distance calculated from the Apoferritin concentration $a_{conc}=18.9$ nm.

The fit values of the thermal displacement Δa_2 are found to be almost independent of polymer concentration which is reasonable since the measurements were carried out at identical temperature. The deviation from the crystalline order Δa_1 increased from 1.8 to 2.5 nm with decreasing polyion concentration due to decreasing electrostatic interactions with increasing distance between macroions.

Since the SAXS data are often interpreted on the basis of the peak position, we analyzed this problem in more details in Fig. 19. For a well pronounced SAXS peak of a low salt sample (237 mg/ml at 0.01 mM NaCl) we plotted all important functions: scattering curve $I(q)$, form factor $F^2(q)$,

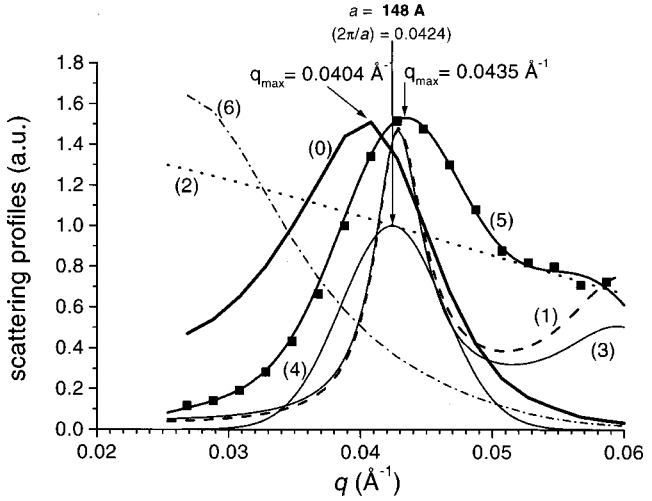

FIG. 19. Detailed analysis of the SAXS data obtained for 237 mg/ml Apoferritin solution at 0.01 mM NaCl. The symbols correspond to the experimental structure factor profile. The solid lines represent: 0—measured scattering curve $I(q)$; $1-h_1(q)$ calculated from Eq. (14) but without the Debye–Waller factor $\exp(-q^2\Delta a_2^2)$; 2—the Debye–Waller factor: $\exp(-q^2\Delta a_2^2)$; 3—$h_1(q)$ calculated from Eq. (14) (product of 1 and 2); 4—$h_2(q)$ calculated from Eq. (15) using $q_{\max}$ corresponding to the fitted value of a; 5—convolution of $h_1(q)$ and $h_2(q)$ calculated using the best fit parameters ($a=149$ Å, $\Delta a_1=18$ Å, $\Delta a_2=15$ Å); 6—measured Apoferritin form factor (high salt data).

structure factor $S(q)=I(q)/F^2(q)$, function $h_1(q)$ [Eq. (14)], function $h_2(q)$ [Eq. (15)] and convolution of $h_1(q)$ and $h_2(q)$. Except $h_2(q)$ which is intentionally placed in the right place, none of the plotted lines exhibit a peak positioned at the q value corresponding to the Bragg condition. The peaks of the two most frequently analyzed functions: $I(q)$ and $S(q)$ lie on the opposite sides of the Bragg condition line (as was already shown in Fig. 15). It seems that the only meaningful parameter defining the peak position is the fitted value of a. For practical reasons, however, one can take as first approximation of $2\pi/a$ the average of the $I(q)$ and $S(q)$ peak positions.

V. CONCLUSIONS

The structure and dynamics of Apoferritin solutions in the dilute regime were studied by means of SAXS and DLS in a wide range of protein concentrations (0.1–237 mg/ml) and added salt content (0.01—100 mM). The Apoferritin sample used in the experiment was very monodisperse what can be seen in the DLS and SAXS data measured at high salt concentrations when the long-range electrostatic interactions are screened. The strength of these interactions present at low and intermediate salt concentrations increases with decreasing salt content and increasing polymer concentration.

As a result of these increasing interactions the dynamics of the polyelectrolyte solution changes in the following way:

(1) The slope of the initial part of the dependence: $D^T=f(c_{\mathrm{Apo}})$ at low polymer concentrations and the plateau value at high concentrations increase according to the predictions of the coupled mode theory. The value of the polyion charge estimated from the CMT analysis seems to be too low, as in most cases.

(2) An additional slow mode appears with increasing relative amplitude and correlation length (decreasing correlation time).

The structure of the polyelectrolyte solution as monitored by means of SAXS reflects the increasing electrostatic interactions by the appearance of a pronounced peak in the structure factor with decreasing width and increasing amplitude. The position of the peak is moving to higher q's with increasing polyion concentration: $q_{\mathrm{Peak}}\propto c_N^{1/3}$, but does not depend on the concentration of added salt at a constant polymer concentration.

The experimental results obtained from a combination of structural (SAXS) and dynamic (DLS) data indicated a direct relationship between the SAXS peak and the slow mode (DLS). These features are the static and dynamic manifestation of the long range ordering of polyions in solutions at intermediate and low ionic strength and they disappear at high salt conditions. The correlation length calculated from the diffusion constant of the slow mode varied between approximately 50 nm (high salt, low-medium Apoferritin concentration) and 100 nm (low salt, high Apoferritin concentration). Using the spatial dimensions of the slow mode as an estimate of the size of the regions with semicrystalline order in the analysis of the SAXS structure factor peak, reasonable results for the fit of the data with the paracrystalline theory of Hosemann and Bagchi are found. Thus, assuming the size of the ordered regions being equal to the correlation length obtained from the slow mode, the degree of spatial ordering within the ordered regions is found to increase in solutions of the same salt content and increasing Apoferritin concentrations. As expected, the disorder increases with increasing salt concentration. In the analysis of all peak data, the thermally induced disorder is found to be constant in agreement with the fact that the measurements were performed at the same temperature.

Since our data indicate that the distance between the macroions obtained from the SAXS peak is practically equal to that calculated from concentration, there is no reason to assume that there exist ordered regions of denser packing (crystalline regions) in our solutions. We do not see any features of such phase separation in our data. We rather interpret our results in the following way: The fast diffusive mode (in the framework of the coupled mode theory) is due to the diffusion of macroions. Electrostatic interactions between macroions induce partial radial order in solution which can be described by a correlation length. The structural representation of this correlation length is the width of the SAXS peak. A dynamic consequence of this correlation length is the slow mode. Hence, the values of this correlation length obtained from static and dynamic measurements should be comparable, as it is really the case.

Thus, we showed that a combination of the two complementary methods of SAXS and DLS can bring new insight into important relationships between the static and dynamic properties of low salt Apoferritin solutions.

ACKNOWLEDGMENTS

The authors wish to thank Professor E. W. Fischer and Professor B. Ewen for supporting this project. Partial financial support of the Bundesministerium für Bildung und Forschung (BMBF Contract No. ME11.07P) is acknowledged. The authors are also grateful to Dr. G. Grübel, P. Feder, and H. Gleyzolle at the beamline ID10A (ESRF, Grenoble), and Dr. G. Meier and Dr. W. Steffen for their support during the USAXS measurements.

[1] H. Liu, L. Skibinska, J. Gapinski, A. Patkowski, E. W. Fischer, and R. Pecora, J. Chem. Phys. **109**, 7556 (1998).
[2] L. Skibinska, J. Gapinski, H. Liu, A. Patkowski, E. W. Fischer, and R. Pecora, J. Chem. Phys. **110**, 1794 (1999).
[3] J. Gapinski, L. Skibinska, H. Liu, A. Patkowski, and R. Pecora, J. Chem. Phys. **113**, 6001 (2000).
[4] A. Patkowski, E. Gulari, and B. Chu, J. Chem. Phys. **73**, 4178 (1980).
[5] A. Patkowski and B. Chu, Biopolymers **18**, 2051 (1979).
[6] A. Patkowski, W. Eimer, J. Seils, G. Schneider, B. M. Jockusch, and Th. Dorfmüller, Biopolymers **30**, 1281 (1990).
[7] J. Moradianoldak, J. P. Simmer, E. C. Lau, T. Diekwisch, H. C. Slavkin, and A. G. Fincham, Connective Tissue Research **32**, 125 (1995).
[8] More on proteins: see R. Pecora, *Dynamic Light Scattering* (Plenum, New York, 1985).
[9] D. N. Petsev and P. G. Vekilov, Biophys. J. **78**, 2060 (2000).
[10] P. M. Harrison and Paolo Arosio, Biochim. Biophys. Acta **1275**, 161 (1996).
[11] T. G. St. Pierre, P. Chan, K. R. Bauchspiess, J. Webb, S. Betteridge, S. Walton, and D. P. E. Dickson, Coord. Chem. Rev. **151**, 125 (1996).
[12] K. S. Kim, H. R. Mun, and J. H. Lee, Inorg. Chim. Acta **298**, 107 (2000).
[13] Ba-Ssalamah, S. Schick, K. Heimberger, K. F. Linnau, N. Schibany, R. Prokesch, and S. Trattnig, Magn. Reson. Imaging **18**, 237 (2000).
[14] G. Bartzokis and T. A. Tishler, Cell. Mol. Biol. Lett. **46**, 821 (2000).
[15] J. M. Domininguez-Vera, D. Rondon, A. Moreno, and J. M. Garcia-Ruiz, J. Cryst. Growth **168**, 138 (1996).
[16] S. H. Kilcoyne, G. R. Mitchell, and R. Cywinski, Physica B **180&181**, 767 (1992).
[17] T. Fujisawa, Y. Inoko, and N. Yagi, J. Synchrotron Radiat. **6**, 1106 (1999).
[18] K. Nagayama, S. Takeda, S. Endo, and H. Yoshimura, Jpn. J. Appl. Phys., Part 1 **34**, 3974 (1995).
[19] S. Takeda, H. Yoshimura, S. Endo, T. Takahaschi, and K. Nagayama, Proteins **23**, 548 (1995).
[20] R. Thomas, D. Carter, and F. Rosenberger, J. Cryst. Growth **187**, 499 (1998).
[21] A. Johnson, Y. Yuan, and A. M. Lenhoff, J. Colloid Interface Sci. **223**, 261 (2000).
[22] N. Petsev and P. G. Vekilov, Phys. Rev. Lett. **84**, 1339 (2000).
[23] T. Alfrey, E. B. Bradford, J. L. Vanderhoff, and G. Oster, J. Opt. Soc. Am. **44**, 603 (1954).
[24] J. Brown, P. N. Pusey, J. W. Goodwin, and R. H. Ottewill, J. Phys. A **8**, 664 (1975).
[25] W. Härtl and H. Versmold, Z. Phys. Chem., Stoechiom. Verwandtschaftsl. **153**, 1 (1987).
[26] J. P. Hansen and J. B. Hayter, Mol. Phys. **46**, 651 (1982).
[27] Svensson and B. Jönsson, Mol. Phys. **50**, 489 (1983).
[28] J.-P. Cotton and M. Moan, J. Phys. (France) Lett. **37**, L75 (1976).
[29] E. Williams, M. Nierlich, J. P. Cotton *et al.*, J. Polym. Sci., Polym. Lett. Ed. **17**, 379 (1979).
[30] M. Drifford, J. P. Dalbiez, K. Tibti, P. Tivant, J. Chim. Phys. Phys.-Chim. Biol **88**, 5368 (1984).
[31] K. Kaji, H. Urakawa, T. Kanaya, and R. Kitamura, J. Phys. (France) **49**, 993 (1988).
[32] M. Nierlich, C. W. Williams, F. Boue *et al.*, J. Phys. (France) **40**, 701 (1979).
[33] N. Ise, T. Okubo, S. Kunigi, H. Matsuoka, K. Yamamoto, and Y. Ishii, J. Chem. Phys. **81**, 3294 (1984).
[34] J. Hayter, G. Janninck, F. Brochard-Wyart, and P. G. de Gennes, J. Phys. (France) Lett. **41**, 451 (1980).
[35] I. Sogami and N. Ise, J. Chem. Phys. **81**, 6320 (1985).
[36] G. Jannink, Makromol. Chem., Macromol. Symp. **1**, 67 (1986).
[37] X. Li and W. F. Reed, J. Chem. Phys. **94**, 4568 (1991).
[38] N. Boudenne and J. Francois, Makromol. Chem. **196**, 3941 (1995).
[39] K. Kassapidou, W. Jesse, M. E. Kuil, A. Lapp, S. Egelhaaf, and J. R. C. Vandermaarel, Macromolecules **30**, 2671 (1997).
[40] M. Milas, M. Rinaudo, R. Duplessix, R. Borsali, and P. Lindner, Macromolecules **28**, 3119 (1995).
[41] R. Rulkens, G. Wegner, and T. Thurn-Albrecht, Langmuir **15**, 4022 (1999).
[42] S. C. Lin, W. I. Lee, and M. J. Schurr, Biopolymers **17**, 1041 (1978).
[43] Ajdari, L. Leibler, and J.-F. Joanny, J. Chem. Phys. **95**, 4580 (1991).
[44] M. Sedlak, J. Chem. Phys. **105**, 10 123 (1996).
[45] R. Berne and R. Pecora, *Dynamic Light Scattering* (Wiley, New York, 1976).
[46] J. Seils and R. Pecora, Macromolecules **25**, 354 (1992).
[47] S. S. Sorlie and R. Pecora, Macromolecules **21**, 1437 (1988).
[48] S. S. Sorlie and R. Pecora, Macromolecules **23**, 487 (1990).
[49] B. J. Ackerson, J. Chem. Phys. **64**, 242 (1976); *ibid.* **69**, 684 (1978).
[50] A. P. Philipse and A. Vrij, J. Chem. Phys. **88**, 6459 (1988).
[51] B. Chu, Q.-C. Ying, F.-J. Yeh, A. Patkowski, W. Steffen, and E. W. Fischer, Langmuir **11**, 1419 (1995).
[52] T. Albrecht, W. Steffen, A. Patkowski, G. Meier, E. W. Fischer, G. Grübel, and D. L. Abernathy, Phys. Rev. Lett. **77**, 5437 (1996).
[53] T. Thurn-Albrecht, G. Meier, P. Müller-Buchbaum *et al.*, Phys. Rev. E **59**, 642 (1999).
[54] A. Evilevitch, V. Lobaskin, U. Olsson, P. Linse, and P. Schurtenberger, Langmuir **17**, 1043 (2001).
[55] G. H. Koenderink, G. A. Vliegenthart, S. G. J. M. Kluijtmans, A. van Blaaderen, A. P. Philipse, and H. N. W. Lekkerker, Langmuir **15**, 4693 (1999).
[56] S. W. Provencher, Comput. Phys. Commun. **27**, 213 (1982).
[57] M. J. Stephen, J. Chem. Phys. **55**, 3878 (1971).
[58] P. Tivant, M. Turq, M. Drifford, R. Magdelenat, and R. Menez, Biopolymers **22**, 643 (1983).
[59] K. Schmitz, Macromolecules **27**, 3442 (1994).
[60] R. Hosemann and S. N. Bagchi, *Direct Analysis of Diffraction by Matter* (North-Holland, Amsterdam, 1962).
[61] H. Matsuoka, H. Tanaka, T. Hashimoto, and N. Ise, Phys. Rev. B **36**, 1754 (1987).
[62] R. W. James, *The Optical Principles of the Diffraction of X-Rays* (Bell, London, 1948).
[63] B. Warren, *X-Ray Diffraction* (Addison-Wesley, Reading, MA, 1969).
[64] G. R. Strobl, Acta Crystallogr., Sect. A: Cryst. Phys., Diffr., Theor. Gen. Crystallogr. **A26**, 367 (1970).
[65] J. S. Pedersen, Adv. Colloid Interface Sci. **70**, 171 (1997).
[66] K. K. W. Wong, T. Douglas, S. Gider, D. D. Awschalom, and S. Mann, Chem. Mater. **10**, 279 (1998).
[67] *Dynamic Light Scattering: The Method and Some Applications*, edited by W. Brown (Clarendon, Oxford, 1993).
[68] B. Carrasco and J. Garcia de la Torre, Biophys. J. **76**, 3044 (1999).
[69] E. Banachowicz, J. Gapinski, and A. Patkowski, Biophys. J. **78**, 70 (2000).